Acta Cryst E CRYSTALLOGRAPHIC COMMUNICATIONS

ISSN 2056-9890

Bis{4-methylbenzyl 2-[4-(propan-2-yl)benzylidene]hydrazinecarbodithioato-κ^2N^2,S}nickel(II): crystal structure and Hirshfeld surface analysis

Enis Nadia Md Yusof,[a] Thahira B. S. A. Ravoof,[a]‡ Mohamed I. M. Tahir,[a] Mukesh M. Jotani[b] and Edward R. T. Tiekink[c]*

[a]Department of Chemistry, Faculty of Science, Universiti Putra Malaysia, 43400, UPM Serdang, Selangor Darul Ehsan, Malaysia, [b]Department of Physics, Bhavan's Sheth R. A. College of Science, Ahmedabad, Gujarat 380001, India, and [c]Research Centre for Crystalline Materials, School of Science and Technology, Sunway University, 47500 Bandar Sunway, Selangor Darul Ehsan, Malaysia. *Correspondence e-mail: edwardt@sunway.edu.my

Received 11 February 2017
Accepted 13 February 2017

Edited by W. T. A. Harrison, University of Aberdeen, Scotland

‡ Additional correspondence author, e-mail: thahira@upm.edu.my.

Keywords: crystal structure; nickel(II); hydrazine carbodithioate; Hirshfeld surface analysis.

CCDC reference: 1532446

Supporting information: this article has supporting information at journals.iucr.org/e

The complete molecule of the title hydrazine carbodithioate complex, $[Ni(C_{19}H_{21}N_2S_2)_2]$, is generated by the application of a centre of inversion. The Ni^{II} atom is *N*,*S*-chelated by two hydrazinecarbodithioate ligands, which provide a *trans*-N_2S_2 donor set that defines a distorted square-planar geometry. The conformation of the five-membered chelate ring is an envelope with the Ni^{II} atom being the flap atom. In the crystal, *p*-tolyl-C—H$\cdots\pi$(benzene-^{i}Pr), ^{i}Pr-C—H$\cdots\pi$(*p*-tolyl) and π–π interactions [between *p*-tolyl rings with inter-centroid distance = 3.8051 (12) Å] help to consolidate the three-dimensional architecture. The analysis of the Hirshfeld surface confirms the importance of H-atom contacts in establishing the packing.

1. Chemical context

Schiff bases derived from *S*-*R*-dithiocarbazate (*R* = methyl/benzyl/methylbenzyl) and heterocyclic aldehydes or ketones have received much attention in recent years owing to their cytotoxicity (Ali *et al.*, 2002; Beshir *et al.*, 2008; Yusof *et al.*, 2015*a*,*b*), as well as their specific and selective anti-bacterial and anti-fungal properties (Low *et al.*, 2014; Maia *et al.*, 2010; Pavan *et al.*, 2010).

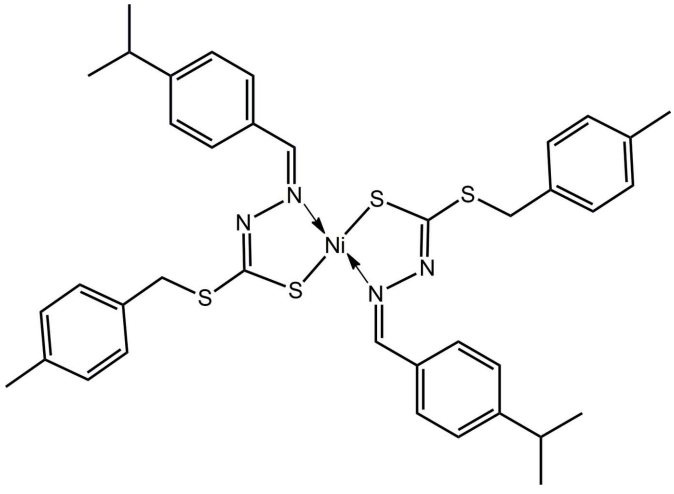

Schiff bases that react with different metal ions often show different types of coordination modes. Metal complexes are versatile molecules with a wide range of pharmacological properties due to the inherent characteristics of both the

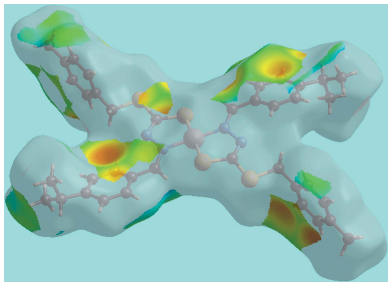

Table 1
Selected bond lengths (Å).

Ni—S1	2.1747 (5)	C1—S2	1.7479 (18)
Ni—N2	1.9137 (15)	C12—S2	1.824 (2)
C1—S1	1.7296 (19)		

central metal atoms and ligands (Meggers, 2009). Various transition metal complexes have been reported to induce DNA cleavage by attacking the sugar or base moieties of DNA through the formation of reactive oxygen species (ROS) (Burrows & Muller, 1998). A nickel(II) bis-dithiocarbazate complex has been used in the photo-catalytic production of hydrogen as a catalyst (Wise *et al.*, 2015). Nickel(II) dithiocarbazate has also been reported to have non-linear optical (NLO) properties (Liu *et al.*, 2016) with the potential to be used in signal processing (Bort *et al.*, 2013; Hales *et al.*, 2014), ultrafast optical communication, data storage, optical limiting (Price *et al.*, 2015; Bouit *et al.*, 2007), optical switching (Gieseking *et al.* 2014; Thorley *et al.*, 2008), logic devices and bio-imaging (Ahn *et al.*, 2012; Zhu *et al.*, 2016). In line with our interest in evaluating the structures of different isomeric dithiocarbazate Schiff bases and their metal complexes, we report herein the synthesis of the title complex, (I), its X-ray crystal structure determination and a detailed study of the supramolecular association by an analysis of its Hirshfeld surface.

2. Structural commentary

The Ni^{II} atom in (I), Fig. 1, is located on a crystallographic centre of inversion and is coordinated by two *S*,*N*-chelating hydrazinecarbodithioate anions. From symmetry, the resulting N_2S_2 donor set has like atoms *trans*, and the square-planar coordination geometry is strictly planar. Distortions from the ideal geometry are related to the deviations of angles subtended at nickel by the donor atoms, Table 1. The C1—N1—N2—C2 backbone of the ligand exhibits a twist as seen in the value of the torsion angle, *i.e.* −165.61 (17)°. Despite being involved in a formal bond to the Ni^{II} atom, the C1—S1 bond

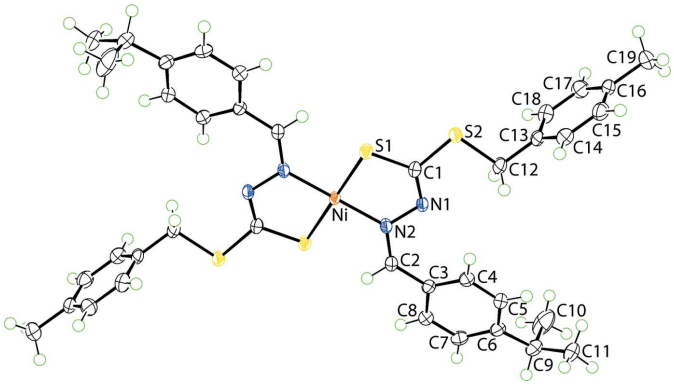

Figure 1
The molecular structure of (I), showing the atom-labelling scheme and displacement ellipsoids at the 70% probability level. The Ni^{II} atom is situated on a centre of inversion. Unlabelled atoms are related by the symmetry operation (1 − *x*, 1 − *y*, 1 − *z*).

Table 2
Hydrogen-bond geometry (Å, °).

*Cg*1 and *Cg*2 are the centroids of the (C3–C8) and (C13–C18) rings, respectively.

D—H···*A*	*D*—H	H···*A*	*D*···*A*	*D*—H···*A*
C2—H2···S1^{i}	0.95	2.48	3.0691 (17)	120
C4—H4···N1	0.95	2.40	2.865 (2)	110
C17—H17···*Cg*1^{ii}	0.95	2.84	3.761 (2)	164
C11—H11*B*···*Cg*2^{iii}	0.98	2.96	3.880 (3)	158

Symmetry codes: (i) $-x+1, -y+1, -z+1$; (ii) $-x, -y, -z+1$; (iii) $x, -y-\frac{3}{2}, z-\frac{1}{2}$.

length of 1.7296 (19) Å is still significantly shorter than those formed by the S2 atom, *i.e.* C1—S2 = 1.7479 (18) Å and C12—S2 = 1.824 (2) Å.

The planarity of the N_2S_2 donor set does not extend to the five-membered chelate ring, which has an envelope conformation with the nickel atom lying 0.465 (2) Å above the least-squares plane through the remaining atoms [r.m.s. deviation = 0.0016 Å]. The sequence of C1═N1, N1—N2 and N2═C2 bond lengths of 1.294 (2), 1.408 (2) and 1.300 (2) Å, respectively, suggests limited conjugation across this residue. Each of the benzene rings of the S- and N-bound substituents is twisted with respect to the least-squares plane through the chelate ring. Thus, a nearly orthogonal relationship exists between the chelate and *p*-tolyl rings, with the dihedral angle

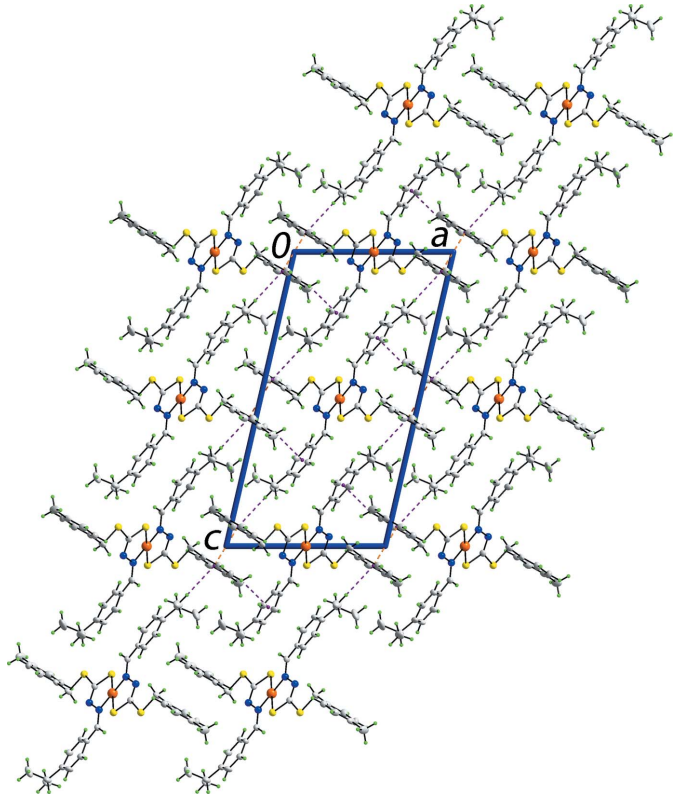

Figure 2
The molecular packing in (I): a view of the unit-cell contents shown in projection down the *b* axis. The *π*–*π* and C—H···*π* interactions are shown as orange and purple dashed lines, respectively.

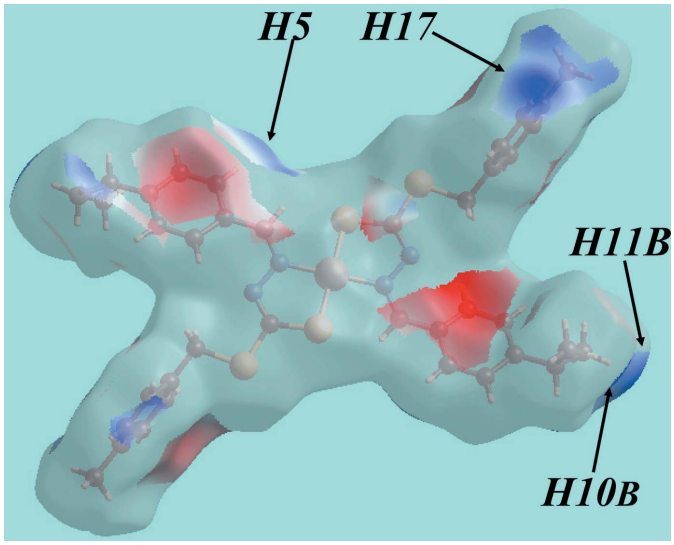

Figure 3
A view of the Hirshfeld surface for (I) mapped over the electrostatic potential over the range ±0.025 au.

being 89.72 (5)°. Less dramatic is the twist of the ^{i}Pr-substituted ring with the dihedral angle being 13.83 (9)°. The dihedral angle between the aromatic rings is 84.31 (6)°.

3. Supramolecular features

The two sites potentially available for hydrogen bonding in (I), *i.e.* the S1 and N1 atoms, are involved in intramolecular interactions, Table 2. The only discernible contacts in the crystal involve π-systems (Spek, 2009). Thus, each of the independent rings is involved in C—H···π contacts, *i.e.* *p*-tolyl-C—H···π(^{i}Pr-benzene) and ^{i}Pr-benzene-C—H···π(*p*-tolyl) contacts, Table 2. In addition, centrosymmetrically related *p*-tolyl rings self-associate *via* face-to-face, π–π, interactions [inter-centroid distance = 3.8051 (12) Å for symmetry operation $-x, -1-y, 1-z$], indicating the *p*-tolyl ring participates in two distinct interactions. The result of the supramolecular association is the formation of a three-dimensional architecture, Fig. 2.

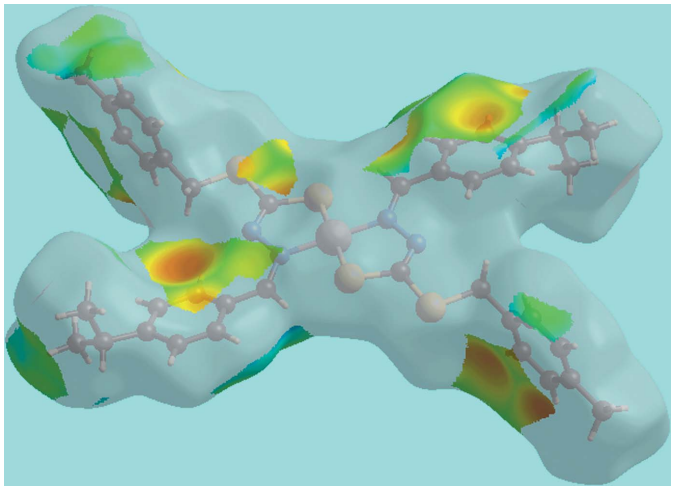

Figure 4
The view of the Hirshfeld surface mapped over d_e. The bright-orange spots near rings indicate their involvement in C—H···π interactions.

4. Analysis of the Hirshfeld surfaces

The Hirshfeld surface analysis for (I) was performed as described in a recent publication of a heavy-atom structure (Mohamad *et al.*, 2017). The non-appearance of characteristic red spots on the Hirshfeld surface mapped over d_{norm} (not shown) clearly indicates the absence of conventional hydrogen bonding in the crystal. The donors and acceptors of C—H···π interactions, involving atoms of each of the ^{i}Pr-benzene and *p*-tolyl rings, are viewed as blue and light-red regions and correspond to the respective positive and negative potentials on the Hirshfeld surface mapped over electrostatic potential (over the range ± 0.025 au), Fig. 3. The acceptors of the C—H···π interactions are also viewed as bright-orange spots

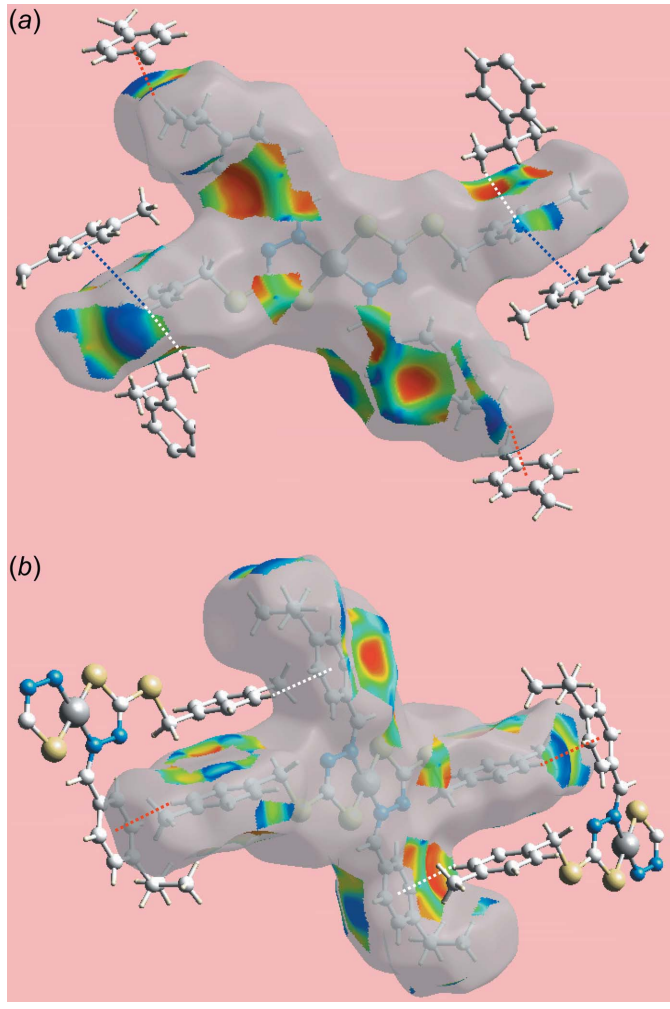

Figure 5
Two views (*a*) and (*b*) of the Hirshfeld surface mapped with shape-index property about a reference molecule. The C—H···π and π···H—C interactions in both views are indicated with red and white dotted lines, respectively. The blue dotted lines in (*a*) indicate π–π stacking between *p*-tolyl rings.

Table 3
Percentage contribution of the different intermolecular contacts to the Hirshfeld surface in (I).

Contact	% contribution
H···H	52.5
C···H/H···C	22.2
S···H/H···S	15.3
N···H/H···N	3.3
C···C	2.1
Ni···H/H···Ni	2.0
S···N/N···S	1.8
C···S/S···C	0.4
S···S	0.3
C···N/N···C	0.1

appearing near ^{i}Pr-benzene and *p*-tolyl rings on the Hirshfeld surface mapped over d_e, Fig. 4. The immediate environment about a reference molecule within the Hirshfeld surface mapped with shape-index property is illustrated in Fig. 5. The C—H···π and their reciprocal contacts, *i.e.* π···H—C contacts, between ^{i}Pr–H11*B* and the *p*-tolyl ring are represented by red and white dotted lines, respectively in Fig. 5*a*; the blue dotted lines in Fig. 5*a* represent π–π stacking between *p*-tolyl rings at $-x$, $-1-y$, $1-z$. The other C—H···π

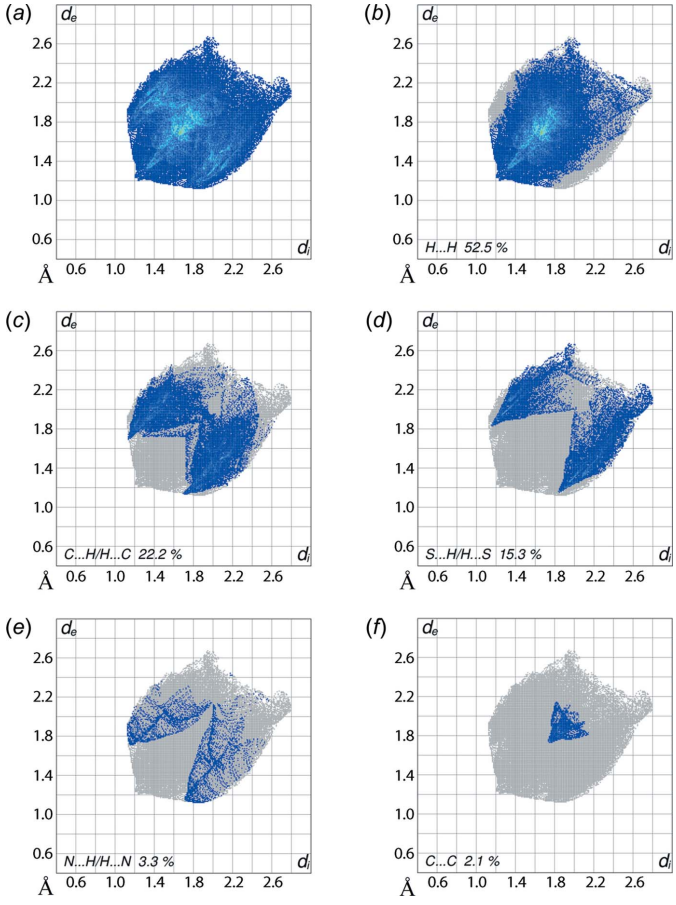

Figure 6
The two-dimensional fingerprint plots for (I): (*a*) all interactions, and delineated into (*b*) H···H, (*c*) C···H/H···C, (*d*) S···H/H···S, (*e*) N···H/H···N and (*f*) C···C interactions.

Table 4
Short interatomic contacts in (I).

Contact	distance	symmetry operation
C16···H10*B*	2.84	$x, -\frac{1}{2}-y, -\frac{1}{2}+z$
C19···H5	2.88	$-x, -1-y, 1-z$

contacts involving *p*-tolyl-H17 and ^{i}Pr-benzene rings are illustrated in Fig. 5*b*.

The overall two-dimensional fingerprint plot and those delineated into H···H, C···H/H···C, S···H/H···S and N···H/H···N and C···C contacts (McKinnon *et al.*, 2007) illustrated in Fig. 6*a–f*. From the quantitative summary of the relative contributions of the various interatomic contacts given in Table 3, it is important to note the dominant contribution of hydrogen atoms to the Hirshfeld surface, *i.e.* 95.3%. In the fingerprint plot delineated into H···H contacts. Fig. 6*b*, the points are distributed in the major part of the plot, but they do not make significant contributions to the molecular packing as their interatomic separations are greater than sum of their van der Waals radii, *i.e.* $d_e + d_i > 2.4$ Å. The presence of short interatomic C···H/H···C contacts, see Table 4, and C—H···π interactions contribute to the second largest contribution to the Hirshfeld surface, *i.e.* 22.2%. This is consistent with the fingerprint plot, Fig. 6*c*, where the short interatomic C···H/H···C contacts appear as a pair of small peaks at $d_e + d_i \sim 2.8$ Å and also as the blue regions around the participating hydrogen atoms, namely H5 and H10*B*, on the Hirshfeld surface mapped over electrostatic potential, Fig. 3. The involvement of the chelating S1 and N1 atoms in intramolecular interactions, Table 2, prevents them from forming intermolecular S···H/H···S and N···H/H···N contacts. However, the symmetrical distribution of points with the usual characteristics in their respective plots, Fig. 6*d* and *e*, indicate meaningful contributions to the Hirshfeld surface, Table 3. A small, *i.e.* 2.1%, but recognizable contribution from C···C contacts to the Hirshfeld surface is ascribed to π–π stacking interactions between symmetry-related *p*-tolyl rings, and appear as an arrow-like distribution of points around

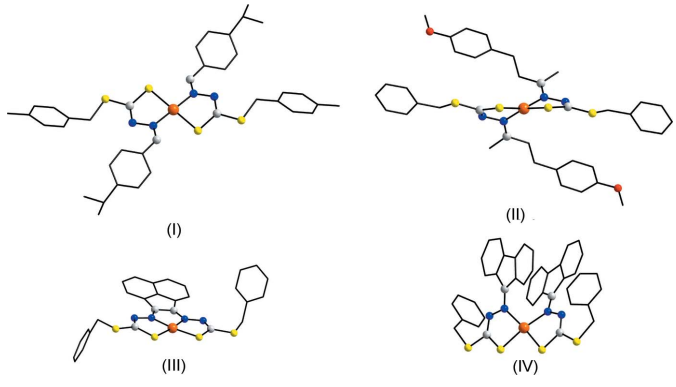

Figure 7
Simplified molecular structure diagrams of (I)–(IV). All C atoms, except those of the C—N—N—C backbone, are represented as small black spheres and H atoms have been omitted.

$d_e = d_i$ 1.9 Å in Fig. 6*f*. The other contacts have low percentage contributions to the surface and are likely to have negligible effects on the molecular packing, Table 3.

5. Database survey

There are three closely related nickel(II) dithiocarbazate complexes in the crystallographic literature (Groom *et al.*, 2016); these are illustrated in simplified form in Fig. 7. Complex (II) differs from (I) only in the nature of the terminal substituents (Tan *et al.*, 2012). Despite there being only small differences in chemical composition, a distinct coordination geometry is observed, with the Ni^{II} atom located on a twofold rotation axis and the N_2S_2 donor set having *cis*-dispositions of like atoms. In (III), with a formal link between the two imine functionalities, the *cis*-N_2S_2 arrangement is imposed by the geometric requirements of the bis(dithiocarbazate) di-anion (Zhou *et al.*, 2002). The molecular structure of (IV), again with a *cis*-N_2S_2 donor set, appears to indicate that steric effects do not preclude a *cis*-N_2S_2 coordination geometry (Liu *et al.*, 2000). With the foregoing in mind, it appears that the molecular structure of (I) is unprecedented, suggesting further systematic investigations in this area are warranted.

6. Synthesis and crystallization

The *S*-4-methylbenzyldithiocarbazate (S4MDTC) precursor was synthesized by following a procedure adapted from the literature (Omar *et al.*, 2014). The Schiff base was also synthesized using a procedure adapted from the literature (Yusof *et al.*, 2015*b*) by the reaction of S4MDTC (2.12 g, 0.01 mol), dissolved in hot acetonitrile (100 ml), with an equimolar amount of 4-isopropylbenzaldehyde (1.48 g, 0.01 mol) in absolute ethanol (20 ml). The mixture was then heated at 353 K until half of the mixture solution reduced and allowed to cool to room temperature until a precipitate formed. The compound was recrystallized from ethanol solution and dried over silica gel.

The synthesized Schiff base (0.33 g, 1 mmol) was dissolved in hot acetonitrile (50 ml) and added to nickel(II) acetate tetrahydrate (0.13 g, 0.5 mmol) in an ethanolic solution (30 ml). The mixture was heated and stirred to reduce the volume of the solution. Precipitation occurred once the mixture cooled to room temperature. The precipitate then was filtered and dried over silica gel. The complex was recrystallized from its methanol solution. Brown prismatic crystals were formed from the filtrate after being left to stand for a month. The crystals were filtered and washed with absolute ethanol at room temperature. Yield: 70%. M.p.: 479–480 K. Elemental composition calculated for $C_{38}H_{42}N_4NiS_4$: C, 61.53; H, 5.71; N, 7.55. Found: C, 61.67; H, 5.87; N, 7.55%. FT–IR (ATR, cm^{-1}): 1589, ν(C═N); 997, ν(N—N); 823, ν(C═S).

7. Refinement

Crystal data, data collection and structure refinement details are summarized in Table 5. The carbon-bound H-atoms were placed in calculated positions (C—H = 0.95–0.99 Å) and were included in the refinement in the riding-model approximation, with U_{iso}(H) set to 1.2–1.5U_{eq}(C).

Table 5
Experimental details.

Crystal data	
Chemical formula	$[Ni(C_{19}H_{21}N_2S_2)_2]$
M_r	741.70
Crystal system, space group	Monoclinic, $P2_1/c$
Temperature (K)	100
a, *b*, *c* (Å)	11.5799 (7), 7.3910 (3), 21.9848 (16)
β (°)	103.033 (7)
V (Å^3)	1833.1 (2)
Z	2
Radiation type	Mo $K\alpha$
μ (mm^{-1})	0.79
Crystal size (mm)	0.30 × 0.20 × 0.10
Data collection	
Diffractometer	Agilent Xcalibur Eos Gemini
Absorption correction	Multi-scan (*CrysAlis PRO*; Agilent, 2011)
T_{min}, T_{max}	0.895, 1.000
No. of measured, independent and observed [$I > 2\sigma(I)$] reflections	8467, 4192, 3393
R_{int}	0.030
(sin $\theta/\lambda)_{max}$ (Å^{-1})	0.674
Refinement	
$R[F^2 > 2\sigma(F^2)]$, $wR(F^2)$, S	0.035, 0.085, 1.02
No. of reflections	4192
No. of parameters	217
H-atom treatment	H-atom parameters constrained
$\Delta\rho_{max}$, $\Delta\rho_{min}$ (e Å^{-3})	0.48, −0.24

Computer programs: *CrysAlis PRO* (Agilent, 2011), *SHELXS97* (Sheldrick, 2008), *SHELXL2014* (Sheldrick, 2015), *ORTEP-3 for Windows* (Farrugia, 2012), *DIAMOND* (Brandenburg, 2006) and *publCIF* (Westrip, 2010).

Acknowledgements

We thank the Department of Chemistry, Universiti Putra Malaysia (UPM), for access to facilities. This research was funded by UPM and the Malaysian Government under the Malaysian Fundamental Research Grant Scheme (FRGS No. 01-01-16-1833FR) and Geran Penyelidikan-Inisiatif Putra Siswazah (GP-IPS No. 9504600). ENMY also wishes to acknowledge the MyPhD programme (MyBrain15) for the award of a Malaysian Government Scholarship.

Funding information

Funding for this research was provided by: Malaysian Fundamental Research Grant Scheme (award No. FRGS No. 01-01-16-1833FR); Geran Penyelidikan-Inisiatif Putra Siswazah (award No. GP-IPS No. 9504600).

References

Agilent (2011). *CrysAlis PRO*. Agilent Technologies, Yarnton, England.

Ahn, H. Y., Yao, S., Wang, X. & Belfield, K. D. (2012). *Appl. Mater. Interfaces*, **4**, 2847–2854.

Ali, M. A., Mirza, A. H., Butcher, R. J., Tarafder, M. T. H., Keat, T. B. & Ali, A. M. (2002). *J. Inorg. Biochem.* **92**, 141–148.

Beshir, A. B., Guchhait, S. K., Gascón, J. A. & Fenteany, G. (2008). *Bioorg. Med. Chem. Lett.* **18**, 498–504.
Bort, G., Gallavardin, T., Ogden, D. & Dalko, P. I. (2013). *Angew. Chem. Int. Ed.* **52**, 4526–4537.
Bouit, P. A., Wetzel, G., Berginc, G., Loiseaux, B., Toupet, L., Feneyrou, P., Bretonnière, Y., Kamada, K., Maury, O. & Andraud, C. (2007). *Chem. Mater.* **19**, 5325–5335.
Brandenburg, K. (2006). *DIAMOND*. Crystal Impact GbR, Bonn, Germany.
Burrows, C. J. & Muller, J. G. (1998). *Chem. Rev*. **98**, 1109–1152.
Farrugia, L. J. (2012). *J. Appl. Cryst.* **45**, 849–854.
Gieseking, R. L., Mukhopadhyay, S., Risko, C. & Brédas, J. L. (2014). *ACS Photonics*, **1**, 261–269.
Groom, C. R., Bruno, I. J., Lightfoot, M. P. & Ward, S. C. (2016). *Acta Cryst.* B**72**, 171–179.
Hales, J. M., Barlow, S., Kim, H., Mukhopadhyay, S., Brédas, J. L., Perry, J. W. & Marder, S. R. (2014). *Chem. Mater.* **26**, 549–560.
Liu, Z.-H., Duan, C.-Y., Li, J.-H., Liu, Y.-J., Mei, Y.-H. & You, X.-Z. (2000). *New J. Chem*. **24**, 1057–1062.
Liu, X., Xiao, Z., Huang, A., Wang, W., Zhang, L., Wang, R. & Sun, D. (2016). *New J. Chem.* **40**, 5957–5965.
Low, M. L., Maigre, L., Dorlet, P., Guillot, R., Pagès, J., Crouse, K. A., Policar, C. & Delsuc, N. (2014). *Bioconjugate Chem.* **25**, 2269–2284.
Maia, P. I. da S., Fernandes, A. G. de A., Silva, J. J. N., Andricopulo, A. D., Lemos, S. S., Lang, E. S., Abram, U. & Deflon, V. M. (2010). *J. Inorg. Biochem.* **104**, 1276–1282.
McKinnon, J. J., Jayatilaka, D. & Spackman, M. A. (2007). *Chem. Commun*. pp. 3814–3816.
Meggers, E. (2009). *Chem. Commun.* pp. 1001–1010.
Mohamad, R., Awang, N., Kamaludin, N. F., Jotani, M. M. & Tiekink, E. R. T. (2017). *Acta Cryst.* E**73**, 260–265.
Omar, S. A., Ravoof, T. B., Tahir, M. I. M. & Crouse, K. A. (2014). *Transition Met. Chem.* **39**, 119–126.
Pavan, F. R., Maia, P. I. da S., Leite, S. R. A., Deflon, V. M., Batista, A. A., Sato, D. N., Franzblau, S. G. & Leite, C. Q. F. (2010). *Eur. J. Med. Chem.* **45**, 1898–1905.
Price, R. S., Dubinina, G., Wicks, G., Drobizhev, M., Rebane, A. & Schanze, K. S. (2015). *Appl. Mater. Interfaces*, **7**, 10795–10805.
Sheldrick, G. M. (2008). *Acta Cryst.* A**64**, 112–122.
Sheldrick, G. M. (2015). *Acta Cryst.* C**71**, 3–8.
Spek, A. L. (2009). *Acta Cryst.* D**65**, 148–155.
Tan, M.-Y., Ravoof, T. B. S. A., Tahir, M. I. M., Crouse, K. A. & Tiekink, E. R. T. (2012). *Acta Cryst.* E**68**, m725–m726.
Thorley, K. J., Hales, J. M., Anderson, H. L. & Perry, J. W. (2008). *Angew. Chem. Int. Ed.* **47**, 7095–7098.
Westrip, S. P. (2010). *J. Appl. Cryst.* **43**, 920–925.
Wise, C. F., Liu, D., Mayer, K. J., Crossland, P. M., Hartley, C. L. & McNamara, W. R. (2015). *Dalton Trans.* **44**, 14265–14271.
Yusof, E. N. Md., Ravoof, T. B. S. A., Jamsari, J., Tiekink, E. R. T., Veerakumarasivam, A., Crouse, K. A., Tahir, M. I. M. & Ahmad, H. (2015*a*). *Inorg. Chim. Acta*, **438**, 85–93.
Yusof, E. N. Md., Ravoof, T. B. S. A., Tiekink, E. R. T., Veerakumarasivam, A., Crouse, K. A., Tahir, M. M. I. & Ahmad, H. (2015*b*). *Int. J. Mol. Sci.* **16**, 11034–11054.
Zhou, J.-H., Wang, Y.-X., Chen, X.-T., Song, Y.-L., Weng, L.-H. & You, X.-Z. (2002). *Chin. J. Inorg. Chem*. **18**, 533–536.
Zhu, Z., Qian, J., Zhao, X., Qin, W., Hu, R., Zhang, H., Li, D., Xu, Z., Tang, B. Z. & He, S. (2016). *ACS Nano*, **10**, 588–597.

supporting information

Acta Cryst. (2017). E**73**, 397-402 [https://doi.org/10.1107/S2056989017002419]

Bis{4-methylbenzyl 2-[4-(propan-2-yl)benzylidene]hydrazinecarbodithioato-κ^2N^2,S}nickel(II): crystal structure and Hirshfeld surface analysis

Enis Nadia Md Yusof, Thahira B. S. A. Ravoof, Mohamed I. M. Tahir, Mukesh M. Jotani and Edward R. T. Tiekink

Computing details

Data collection: *CrysAlis PRO* (Agilent, 2011); cell refinement: *CrysAlis PRO* (Agilent, 2011); data reduction: *CrysAlis PRO* (Agilent, 2011); program(s) used to solve structure: *SHELXS97* (Sheldrick, 2008); program(s) used to refine structure: *SHELXL2014* (Sheldrick, 2015); molecular graphics: *ORTEP-3 for Windows* (Farrugia, 2012) and *DIAMOND* (Brandenburg, 2006); software used to prepare material for publication: *publCIF* (Westrip, 2010).

Bis{4-methylbenzyl 2-[4-(propan-2-yl)benzylidene]hydrazinecarbodithioato-κ^2N^2,S}nickel(II):

Crystal data

$[Ni(C_{19}H_{21}N_2S_2)_2]$
M_r = 741.70
Monoclinic, $P2_1/c$
a = 11.5799 (7) Å
b = 7.3910 (3) Å
c = 21.9848 (16) Å
β = 103.033 (7)°
V = 1833.1 (2) Å^3
Z = 2
$F(000)$ = 780
D_x = 1.344 Mg m^{-3}
Mo $K\alpha$ radiation, λ = 0.7107 Å
Cell parameters from 3077 reflections
θ = 2.3–28.7°
μ = 0.79 mm^{-1}
T = 100 K
Prism, brown
0.30 × 0.20 × 0.10 mm

Data collection

Agilent Xcalibur Eos Gemini diffractometer
Radiation source: Enhance (Mo) X-ray Source
Graphite monochromator
Detector resolution: 16.1952 pixels mm^{-1}
ω scans
Absorption correction: multi-scan (CrysAlis PRO; Agilent, 2011)
T_{min} = 0.895, T_{max} = 1.000
8467 measured reflections
4192 independent reflections
3393 reflections with $I > 2\sigma(I)$
R_{int} = 0.030
θ_{max} = 28.6°, θ_{min} = 2.3°
h = −15→14
k = −9→9
l = −27→29

Refinement

Refinement on F^2
Least-squares matrix: full
$R[F^2 > 2\sigma(F^2)]$ = 0.035
$wR(F^2)$ = 0.085
S = 1.02
4192 reflections
217 parameters
0 restraints
Primary atom site location: structure-invariant direct methods
Hydrogen site location: inferred from neighbouring sites
H-atom parameters constrained
$w = 1/[\sigma^2(F_o^2) + (0.0367P)^2 + 0.7493P]$ where $P = (F_o^2 + 2F_c^2)/3$
$(\Delta/\sigma)_{max}$ = 0.001

$\Delta\rho_{max}$ = 0.48 e Å^{-3} $\Delta\rho_{min}$ = −0.24 e Å^{-3}

Special details

Geometry. All esds (except the esd in the dihedral angle between two l.s. planes) are estimated using the full covariance matrix. The cell esds are taken into account individually in the estimation of esds in distances, angles and torsion angles; correlations between esds in cell parameters are only used when they are defined by crystal symmetry. An approximate (isotropic) treatment of cell esds is used for estimating esds involving l.s. planes.

Fractional atomic coordinates and isotropic or equivalent isotropic displacement parameters (Å^2)

	x	*y*	*z*	U_{iso}*/U_{eq}
Ni	0.5000	0.5000	0.5000	0.01242 (9)
S1	0.46625 (4)	0.27399 (6)	0.43507 (2)	0.01691 (12)
S2	0.29415 (4)	−0.01653 (6)	0.43496 (2)	0.01892 (12)
N1	0.36782 (13)	0.1991 (2)	0.53197 (7)	0.0153 (3)
N2	0.43911 (13)	0.3485 (2)	0.55606 (7)	0.0141 (3)
C1	0.37730 (16)	0.1603 (2)	0.47593 (9)	0.0150 (4)
C2	0.45497 (16)	0.3715 (2)	0.61599 (9)	0.0156 (4)
H2	0.5057	0.4692	0.6325	0.019*
C3	0.40706 (16)	0.2706 (2)	0.66191 (9)	0.0158 (4)
C4	0.37058 (16)	0.0885 (3)	0.65720 (9)	0.0173 (4)
H4	0.3835	0.0158	0.6237	0.021*
C5	0.31580 (17)	0.0154 (3)	0.70149 (9)	0.0191 (4)
H5	0.2931	−0.1084	0.6981	0.023*
C6	0.29286 (17)	0.1173 (3)	0.75084 (9)	0.0192 (4)
C7	0.33687 (18)	0.2946 (3)	0.75775 (9)	0.0215 (4)
H7	0.3273	0.3649	0.7925	0.026*
C8	0.39416 (17)	0.3687 (3)	0.71472 (9)	0.0197 (4)
H8	0.4252	0.4879	0.7210	0.024*
C9	0.21599 (19)	0.0493 (3)	0.79346 (10)	0.0247 (5)
H9	0.2445	0.1068	0.8353	0.030*
C10	0.0885 (2)	0.1130 (4)	0.76693 (13)	0.0426 (7)
H10A	0.0864	0.2455	0.7655	0.064*
H10B	0.0371	0.0696	0.7937	0.064*
H10C	0.0604	0.0646	0.7247	0.064*
C11	0.2185 (2)	−0.1560 (3)	0.80247 (11)	0.0298 (5)
H11A	0.1814	−0.2148	0.7629	0.045*
H11B	0.1749	−0.1879	0.8343	0.045*
H11C	0.3009	−0.1968	0.8159	0.045*
C12	0.21972 (18)	−0.1039 (3)	0.49369 (9)	0.0202 (4)
H12A	0.2782	−0.1605	0.5283	0.024*
H12B	0.1800	−0.0041	0.5110	0.024*
C13	0.12954 (16)	−0.2422 (3)	0.46281 (9)	0.0167 (4)
C14	0.15875 (17)	−0.4252 (3)	0.46395 (9)	0.0195 (4)
H14	0.2363	−0.4633	0.4841	0.023*
C15	0.07536 (19)	−0.5521 (3)	0.43589 (10)	0.0227 (4)
H15	0.0966	−0.6764	0.4372	0.027*
C16	−0.03838 (18)	−0.5005 (3)	0.40599 (10)	0.0212 (4)
C17	−0.06739 (17)	−0.3171 (3)	0.40435 (10)	0.0230 (4)

H17	−0.1447	−0.2791	0.3838	0.028*
C18	0.01567 (17)	−0.1900 (3)	0.43244 (10)	0.0211 (4)
H18	−0.0054	−0.0656	0.4309	0.025*
C19	−0.1304 (2)	−0.6381 (3)	0.37581 (11)	0.0329 (5)
H19A	−0.1946	−0.6411	0.3982	0.049*
H19B	−0.0936	−0.7580	0.3775	0.049*
H19C	−0.1626	−0.6045	0.3322	0.049*

Atomic displacement parameters (Å²)

	U^{11}	U^{22}	U^{33}	U^{12}	U^{13}	U^{23}
Ni	0.01367 (16)	0.01287 (16)	0.01220 (17)	−0.00309 (12)	0.00605 (13)	−0.00017 (13)
S1	0.0214 (2)	0.0164 (2)	0.0156 (2)	−0.00518 (18)	0.00956 (19)	−0.00249 (19)
S2	0.0239 (2)	0.0188 (2)	0.0157 (2)	−0.00893 (18)	0.0080 (2)	−0.0039 (2)
N1	0.0169 (8)	0.0147 (7)	0.0157 (8)	−0.0057 (6)	0.0062 (6)	−0.0015 (7)
N2	0.0141 (7)	0.0131 (7)	0.0160 (8)	−0.0033 (6)	0.0054 (6)	−0.0013 (6)
C1	0.0160 (9)	0.0122 (8)	0.0174 (9)	−0.0010 (7)	0.0049 (8)	0.0020 (7)
C2	0.0154 (9)	0.0155 (9)	0.0165 (10)	−0.0035 (7)	0.0049 (8)	0.0003 (8)
C3	0.0146 (9)	0.0205 (9)	0.0127 (9)	−0.0035 (7)	0.0037 (7)	0.0012 (8)
C4	0.0185 (9)	0.0198 (9)	0.0144 (9)	−0.0022 (7)	0.0052 (8)	−0.0012 (8)
C5	0.0202 (9)	0.0200 (9)	0.0169 (10)	−0.0057 (7)	0.0040 (8)	0.0018 (8)
C6	0.0187 (9)	0.0255 (10)	0.0133 (9)	−0.0029 (8)	0.0037 (8)	0.0027 (8)
C7	0.0275 (11)	0.0258 (10)	0.0126 (9)	−0.0035 (8)	0.0074 (8)	−0.0033 (8)
C8	0.0218 (10)	0.0214 (10)	0.0159 (10)	−0.0051 (8)	0.0040 (8)	0.0001 (8)
C9	0.0275 (11)	0.0317 (11)	0.0167 (10)	−0.0059 (9)	0.0089 (9)	0.0021 (9)
C10	0.0313 (13)	0.0582 (17)	0.0461 (16)	0.0062 (11)	0.0250 (12)	0.0199 (14)
C11	0.0330 (12)	0.0345 (12)	0.0240 (11)	−0.0100 (10)	0.0109 (10)	0.0080 (10)
C12	0.0232 (10)	0.0227 (10)	0.0173 (10)	−0.0079 (8)	0.0101 (8)	−0.0014 (8)
C13	0.0170 (9)	0.0199 (9)	0.0156 (9)	−0.0052 (7)	0.0086 (8)	−0.0010 (8)
C14	0.0199 (10)	0.0203 (9)	0.0189 (10)	0.0007 (8)	0.0059 (8)	0.0015 (8)
C15	0.0326 (11)	0.0165 (9)	0.0207 (10)	−0.0021 (8)	0.0094 (9)	0.0000 (8)
C16	0.0260 (10)	0.0230 (10)	0.0159 (10)	−0.0113 (8)	0.0074 (8)	−0.0010 (8)
C17	0.0155 (9)	0.0301 (11)	0.0225 (11)	−0.0019 (8)	0.0025 (8)	0.0032 (9)
C18	0.0222 (10)	0.0174 (9)	0.0251 (11)	−0.0004 (8)	0.0080 (9)	0.0024 (9)
C19	0.0376 (13)	0.0351 (12)	0.0251 (12)	−0.0209 (10)	0.0051 (10)	−0.0034 (10)

Geometric parameters (Å, º)

Ni—S1	2.1747 (5)	C9—H9	1.0000
Ni—N2	1.9137 (15)	C10—H10A	0.9800
Ni—N2^{i}	1.9138 (15)	C10—H10B	0.9800
Ni—S1^{i}	2.1746 (5)	C10—H10C	0.9800
C1—S1	1.7296 (19)	C11—H11A	0.9800
C1—S2	1.7479 (18)	C11—H11B	0.9800
C12—S2	1.824 (2)	C11—H11C	0.9800
N1—C1	1.294 (2)	C12—C13	1.509 (2)
N1—N2	1.408 (2)	C12—H12A	0.9900
N2—C2	1.300 (2)	C12—H12B	0.9900

C2—C3	1.461 (3)	C13—C18	1.391 (3)
C2—H2	0.9500	C13—C14	1.393 (3)
C3—C8	1.405 (3)	C14—C15	1.387 (3)
C3—C4	1.408 (3)	C14—H14	0.9500
C4—C5	1.386 (3)	C15—C16	1.386 (3)
C4—H4	0.9500	C15—H15	0.9500
C5—C6	1.395 (3)	C16—C17	1.395 (3)
C5—H5	0.9500	C16—C19	1.514 (3)
C6—C7	1.401 (3)	C17—C18	1.386 (3)
C6—C9	1.516 (3)	C17—H17	0.9500
C7—C8	1.385 (3)	C18—H18	0.9500
C7—H7	0.9500	C19—H19A	0.9800
C8—H8	0.9500	C19—H19B	0.9800
C9—C11	1.529 (3)	C19—H19C	0.9800
C9—C10	1.534 (3)		

N2—Ni—N2^{i}	180.00 (7)	C9—C10—H10A	109.5
N2—Ni—S1^{i}	93.71 (5)	C9—C10—H10B	109.5
N2^{i}—Ni—S1^{i}	86.29 (5)	H10A—C10—H10B	109.5
N2—Ni—S1	86.30 (5)	C9—C10—H10C	109.5
N2^{i}—Ni—S1	93.70 (5)	H10A—C10—H10C	109.5
S1^{i}—Ni—S1	180.0	H10B—C10—H10C	109.5
C1—S1—Ni	94.14 (6)	C9—C11—H11A	109.5
C1—S2—C12	101.14 (9)	C9—C11—H11B	109.5
C1—N1—N2	111.31 (15)	H11A—C11—H11B	109.5
C2—N2—N1	114.86 (15)	C9—C11—H11C	109.5
C2—N2—Ni	126.01 (13)	H11A—C11—H11C	109.5
N1—N2—Ni	119.11 (12)	H11B—C11—H11C	109.5
N1—C1—S1	125.12 (14)	C13—C12—S2	108.11 (14)
N1—C1—S2	120.09 (14)	C13—C12—H12A	110.1
S1—C1—S2	114.77 (11)	S2—C12—H12A	110.1
N2—C2—C3	130.15 (17)	C13—C12—H12B	110.1
N2—C2—H2	114.9	S2—C12—H12B	110.1
C3—C2—H2	114.9	H12A—C12—H12B	108.4
C8—C3—C4	117.91 (18)	C18—C13—C14	118.53 (17)
C8—C3—C2	115.80 (16)	C18—C13—C12	120.86 (17)
C4—C3—C2	126.26 (18)	C14—C13—C12	120.60 (17)
C5—C4—C3	119.90 (18)	C15—C14—C13	120.43 (18)
C5—C4—H4	120.1	C15—C14—H14	119.8
C3—C4—H4	120.1	C13—C14—H14	119.8
C4—C5—C6	122.24 (18)	C16—C15—C14	121.13 (19)
C4—C5—H5	118.9	C16—C15—H15	119.4
C6—C5—H5	118.9	C14—C15—H15	119.4
C5—C6—C7	117.45 (18)	C15—C16—C17	118.47 (18)
C5—C6—C9	122.87 (18)	C15—C16—C19	121.53 (19)
C7—C6—C9	119.53 (18)	C17—C16—C19	120.00 (19)
C8—C7—C6	120.95 (19)	C18—C17—C16	120.55 (18)
C8—C7—H7	119.5	C18—C17—H17	119.7

C6—C7—H7	119.5	C16—C17—H17	119.7
C7—C8—C3	121.12 (18)	C17—C18—C13	120.87 (18)
C7—C8—H8	119.4	C17—C18—H18	119.6
C3—C8—H8	119.4	C13—C18—H18	119.6
C6—C9—C11	114.35 (18)	C16—C19—H19A	109.5
C6—C9—C10	108.19 (18)	C16—C19—H19B	109.5
C11—C9—C10	110.02 (19)	H19A—C19—H19B	109.5
C6—C9—H9	108.0	C16—C19—H19C	109.5
C11—C9—H9	108.0	H19A—C19—H19C	109.5
C10—C9—H9	108.0	H19B—C19—H19C	109.5

C1—N1—N2—C2	−165.61 (17)	C4—C3—C8—C7	−6.2 (3)
C1—N1—N2—Ni	15.80 (19)	C2—C3—C8—C7	172.25 (17)
N2—N1—C1—S1	0.5 (2)	C5—C6—C9—C11	30.3 (3)
N2—N1—C1—S2	−178.25 (12)	C7—C6—C9—C11	−154.27 (19)
Ni—S1—C1—N1	−12.72 (17)	C5—C6—C9—C10	−92.6 (2)
Ni—S1—C1—S2	166.05 (9)	C7—C6—C9—C10	82.8 (2)
C12—S2—C1—N1	−3.28 (18)	C1—S2—C12—C13	171.91 (13)
C12—S2—C1—S1	177.88 (11)	S2—C12—C13—C18	−86.5 (2)
N1—N2—C2—C3	−2.5 (3)	S2—C12—C13—C14	93.3 (2)
Ni—N2—C2—C3	176.01 (15)	C18—C13—C14—C15	−0.6 (3)
N2—C2—C3—C8	−152.0 (2)	C12—C13—C14—C15	179.55 (19)
N2—C2—C3—C4	26.3 (3)	C13—C14—C15—C16	0.2 (3)
C8—C3—C4—C5	4.7 (3)	C14—C15—C16—C17	0.4 (3)
C2—C3—C4—C5	−173.58 (18)	C14—C15—C16—C19	−179.4 (2)
C3—C4—C5—C6	1.2 (3)	C15—C16—C17—C18	−0.5 (3)
C4—C5—C6—C7	−5.6 (3)	C19—C16—C17—C18	179.2 (2)
C4—C5—C6—C9	169.86 (18)	C16—C17—C18—C13	0.0 (3)
C5—C6—C7—C8	4.1 (3)	C14—C13—C18—C17	0.5 (3)
C9—C6—C7—C8	−171.54 (18)	C12—C13—C18—C17	−179.67 (19)
C6—C7—C8—C3	1.8 (3)		

Symmetry code: (i) −*x*+1, −*y*+1, −*z*+1.

Hydrogen-bond geometry (Å, º)

*Cg*1 and *Cg*2 are the centroids of the (C3–C8) and (C13–C18) rings, respectively.

D—H···*A*	*D*—H	H···*A*	*D*···*A*	*D*—H···*A*
C2—H2···S1^{i}	0.95	2.48	3.0691 (17)	120
C4—H4···N1	0.95	2.40	2.865 (2)	110
C17—H17···*Cg*1^{ii}	0.95	2.84	3.761 (2)	164
C11—H11*B*···*Cg*2^{iii}	0.98	2.96	3.880 (3)	158

Symmetry codes: (i) −*x*+1, −*y*+1, −*z*+1; (ii) −*x*, −*y*, −*z*+1; (iii) *x*, −*y*−3/2, *z*−1/2.